ChemPhysChem

Supporting Information

Structural and Chemical Properties of NiO_x Thin Films: Oxygen Vacancy Formation in O_2 Atmosphere

Raoul Blume,* Wolfram Calvet, Aliakbar Ghafari, Thomas Mayer, Axel Knop-Gericke, and Robert Schlögl

Structural and Chemical Properties of NiO_x Thin Films: Oxygen vacancy formation in O_2 atmosphere

Fit Model and Quantification

$Ni2p_{3/2}$	metal	NiO 1	NiO 2	NiO 3	NiO 4	NiO 5
BE (eV)	852,5	853,75	855,5	861	863,9	866.1 - 866.6
α	0,13					
FWHM (eV)	1,2	1,2	2,8	4 (O_2) / 3.5 (H_2O)	2,3	3,3

O1s	NiO_{1-x}	NiO	Ni_{1-x}-OH	NiOOH	$Ni_2O_3/Ni(OH)_2$	NiOOH	NiO-H_2O_{ad}	H_2O-H_2O
BE (eV) @								
1000 eV	528,9	529,4	529,95	530,6	531,2	531,8	532,7	533,6
880 eV		529,4				531,9		
680 eV		529,4				532		
FWHM (eV)	1	1	1,2	1,2	1,2	1,2	1,2	1,2

SI-Table 1: Fit components and parameter used in the fit model.

Since NiO_x oxide spectra can be prone to charging effects their Binding Energies (BEs) have to be carefully analysed to avoid random shifts to the spectra. The BE of the Ni2p, O1s and VB oxide spectra were calibrated using a multi-step approach. A general outline of this procedure is given in SI-Figure 1. Firstly, the BE of freshly grown NiO_x was determined by referencing to the metal Fermi Edge during oxide growth (SI-Figure 1 a), step 1). This step also delivers the BE references for the Ni2p and O1s regions. Remarkably, the shape of the resulting oxide VB spectrum is almost identical for a) temperatures below ≈ 150°C and b) different photon energies (SI-Figure 1 b). Hence, the BE of the freshly grown oxide VB spectrum was used as a reference to compensate charging effects of all other spectra recorded under similar conditions and photon energies (step 2). In the following step the onset of all VB spectra of each photon energy recorded at different temperatures were carefully adjusted. Since the changes of the spectral features in the VB are closely related to those of the Ni2p region, e.g., as depicted in SI-Figures 4 and 5 and described in the main text, the spectral evolution of the latter was checked to monitor BE consistency. Similarly, this was performed for the O1s spectra recorded at different photon energies. In summary, the described procedure delivers a reliable BE calibration for NiO_x.

For XPS analysis a Shirley-type background correction was applied.[1] Spectra were fitted following the Levenberg-Marquardt algorithm to minimize the standard deviation expressed by the chi-square value χ^2. The peak shapes were adopted by Doniach-Sunjic functions convoluted with Gaussian profiles.[2] This modelling allows for the introduction of an asymmetry factor α where required. SI-Table 1 provides an overview of the Ni2p and O1s deconvolution and the parameters applied. Especially the evaluation of the Ni2p core levels is difficult due to the nature of the photoemission process in nickel oxide and its water related derivatives with various contributions of Ni3d-O2p related photo-hole transitions resulting in a spectral signature with a distinct satellite structure. The Ni2p region fits use the same satellite structure as Biesinger et al.[3,4] FWHM are applied according to the performance of the beamline and the spectrometer. The O1s fits use binding energies according to Fingerle et al.[5] The accuracy of the binding energy position is $\approx \pm 0.05$ eV.

Quantification of the sample composition was performed assuming a homogeneous mixture of Ni and O with $C_x = n_x / \Sigma_i n_i$, with $n_x = I(x) / S_x$ and $S_x = B\ \sigma\ \lambda_{total}$ (λ_{total}: electron escape depth; σ: cross section, B: instrumental contributions) as well as considering the photon flux. S_{Ni} was determined using respective σ and λ_{total} values listed by Yeh et al. and Seah, respectively.[6,7] S_{oxygen} was determined by fitting the spectrum of a freshly prepared NiO and assuming the intensity of the full Ni2p and the O1s NiO component as 1:1 NiO. Note that XPS quantification, with the assumption of a homogeneously mixed composition, is a rather rough approximation and could potentially lead to a systematic error yielding an offset of the Ni and O fractions in NiO. Thus, it should be used as a guideline to follow changes in the composition of the samples presented here. However, quantitative analysis of depth profiles (not shown here) indicates that apart from such off set the compositional changes observed for different depths exhibit the same trends. This not only confirms that the observed results are mostly surface related (see SI-Figure 8) but also allows to estimate an error for these changes (excluding the offset) in the range of only ± 2 - 3 %. Thus, the quantification method applied here correctly reflects the evolution of the sample composition in dependence of temperature.

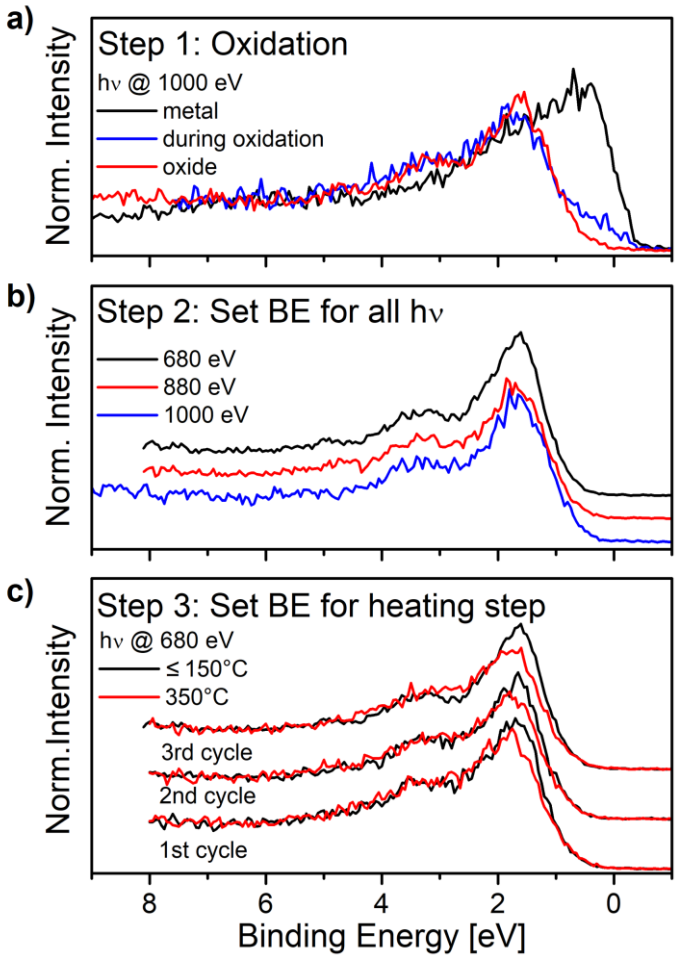

SI-Figure 1: a) VB spectra recorded during the oxidation of a metallic Ni film in 0.5 mbar O_2 atmosphere. b) VB spectra recorded after oxidation at RT and different photon energies. c) Selected VB spectra recorded during heating-cooling cycles in 0.5 mbar O_2 atmosphere corresponding to the 150 and 350°C steps, respectively, displayed in SI-Figure 5 and Figures 4 and 5 of the main text.

Preparation of NiO_x

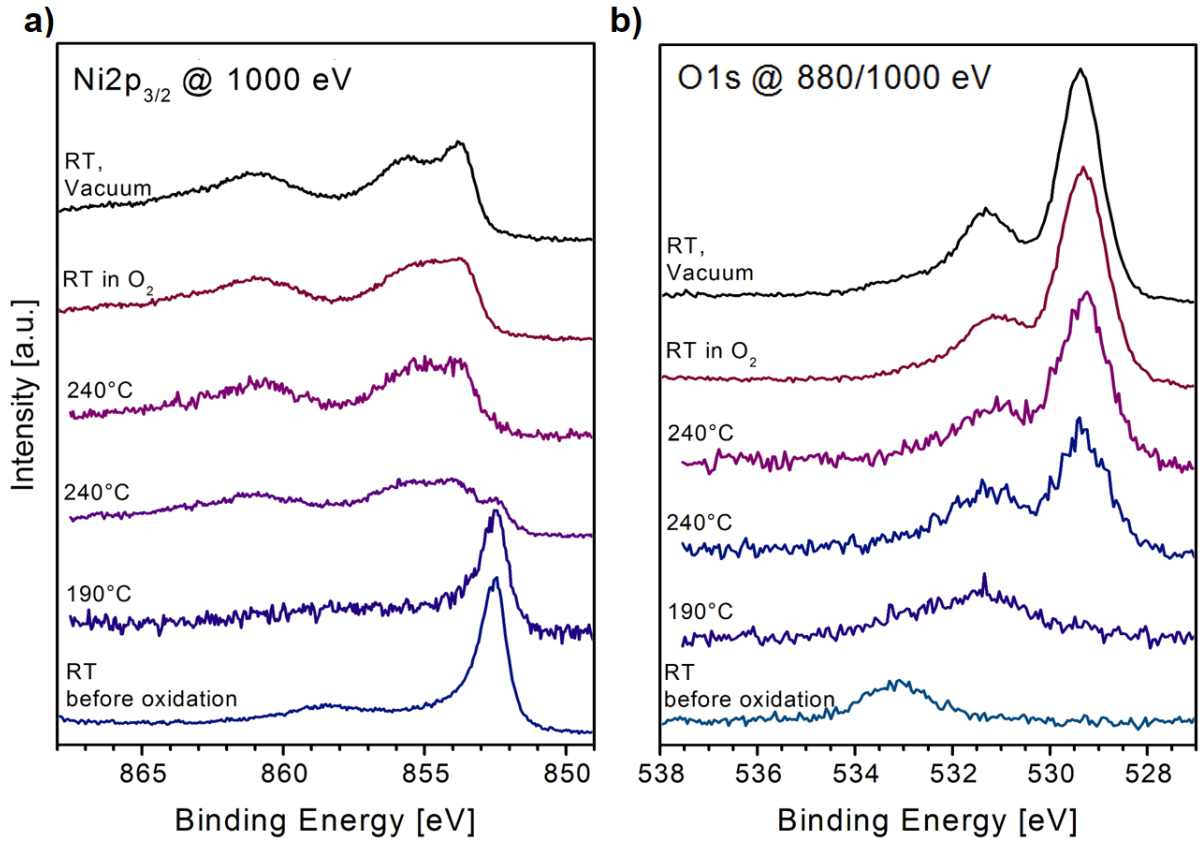

SI-Figure 2: a) XP spectra of the Ni2p3/2 region and b) the O1s region upon oxidizing metallic Ni in 0.5 mbar O_2 atmosphere. Note: The Ni metal spectrum before oxidation is scaled down for better comparison. Note also, that the O1s spectrum at RT in vacuum after oxidation was recorded at 880 eV.

Since the sputtered Ni film was exposed to air on the way to the analysis system, the initial nickel surface was contaminated and partially oxidized at the surface. Hence this native oxide was thermally reduced until the O1s peak was almost gone and a sharp $Ni2p_{3/2}$ peak located at 852.52 eV without any apparent oxide features appeared, indicating a metallic phase. This step is necessary since exposure to air induces the formation of nickel hydroxides and its derivates besides the formation of nickel oxides due to the presence of both, oxygen and water vapour. The reduction of the native oxide as well as the decay of residual carbon species set in between 200 to 250°C. It should be noted that the residual carbon vanishes completely just below 300 °C. This behaviour is attributed to desorption and decay of C-O species followed by graphitization and bulk diffusion of residual carbon.[8,9,10,11] The metallic Ni film was used for the oxidation to contaminant-free NiO by ramping the sample temperature stepwise from RT to ~ 250 °C under 0.5 mbar oxygen induced partial pressure. In SI-Figure 2 a) and b) an exemplary overview of Ni2p and O1s XPS spectra is displayed in the temperature range from 190 to 240 °C in which the oxidation of metallic nickel takes place. The $Ni2p_{3/2}$ and O1s regions after oxidation (top spectra in SI-figure 2) exhibit the typical spectral shapes expected of NiO. In particular, this includes the stepped main intensity and satellite structure of $Ni2p_{3/2}$.[12,13] For further details see the main text.

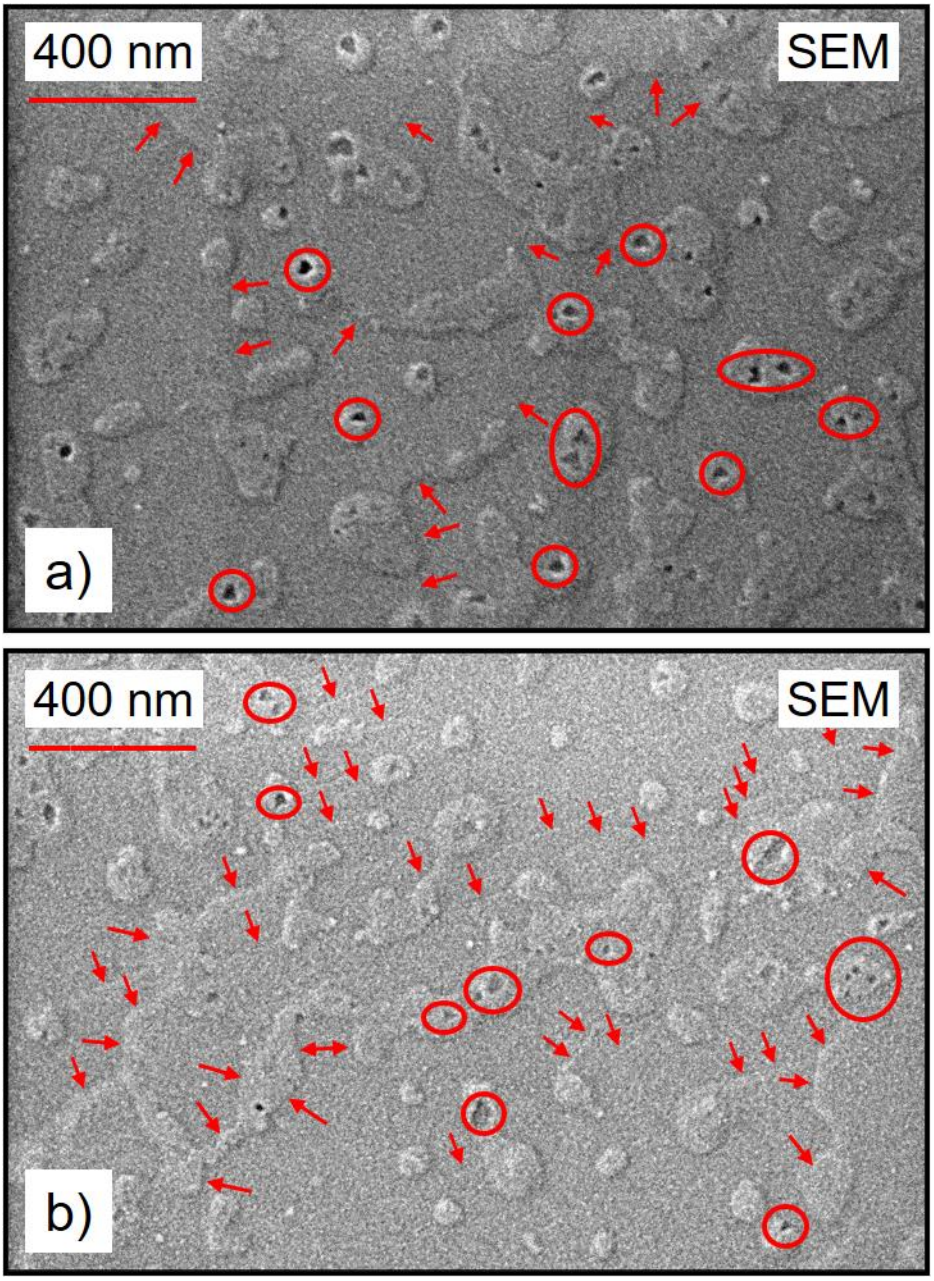

SI-Figure 3: SEM micrographs of a) the as prepared NiO_x sample, b) after three heating-cooling cycles in O_2.

SI-SI-Figure 3 a) and b) depict SEM micrographs of a NiO_x sample before and after three annealing cycles to 350°C and subsequent cooling in 0.5 mbar O_2. The as prepared NiO_x film in SI-Figure 3 a) appears mainly flat with a small number of visible step edges or terraces. Moreover, rather inhomogeneous, protruding areas are present which suggests the presence of more than one surface orientation. On closer inspection, the boundaries of the protruding areas feature some hexagonal and triangular shapes as well as mainly triangular cavities in the center of those areas. The flat sample areas are most likely related to NiO(100) because this represents the most stable NiO orientation.[14,15,16] On the other hand, the hexagonal and triangular shapes of the protruding areas as well as the triangular holes within may indicate the presence of NiO(111). The coexistence of NiO(111) on NiO(100) has been reported before and fits well to XRD data of thin NiO films reported elsewhere.[17,18,19,20,21] The morphology changes after annealing in O_2. The flat sample areas become visibly terraced even detectable with SEM, indicated by red arrows in Figure 3 b). The number of protruding areas seems to

decrease while their remaining areas coagulate predominantly at step edges thus forming a cross-linked structure with elongated extensions that are up to several micrometers long and ~ 50 nm wide. Their boundaries still feature hexagonal and triangular shapes (red circles). This behavior fits to the assignment of these features to NiO(111) which is expected to be unstable above 220 °C and would explain their area loss and coagulation.[15]

Oxygen vacancies on NiO_x up 650°C in O_2 atmosphere

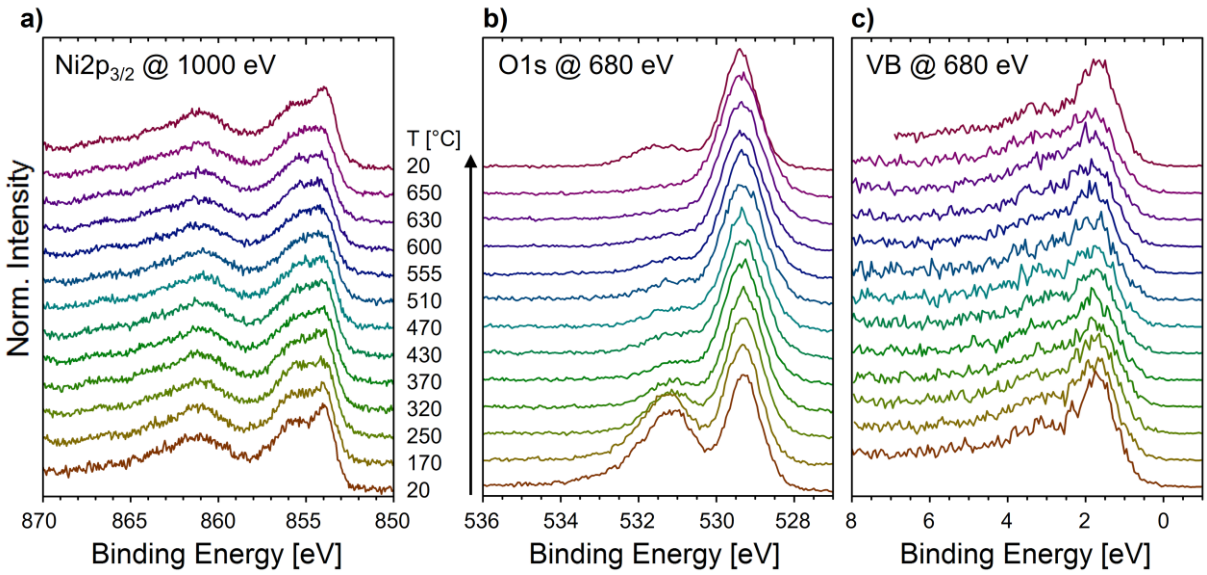

SI-Figure 4: a) Ni $2p_{3/2}$ spectra during heating to 650°C in 0.5 mbar O_2 atmosphere subsequent cooling to RT in vacuum. b) and c) O1s and VB spectra, respectively, corresponding to a). The same color indicates the same temperature in each region.

SI-Figure 4 shows the complete Ni$2p_{3/2}$, O1s and VB data sets recorded during heating of a NiO_x film to 650°C in 0.5 mbar O_2 atmosphere and subsequent cooling to RT in vacuum corresponding to Figures 2 and 3 of the main text.

Formation and replenishing of oxygen vacancies on NiO_x in O_2 atmosphere

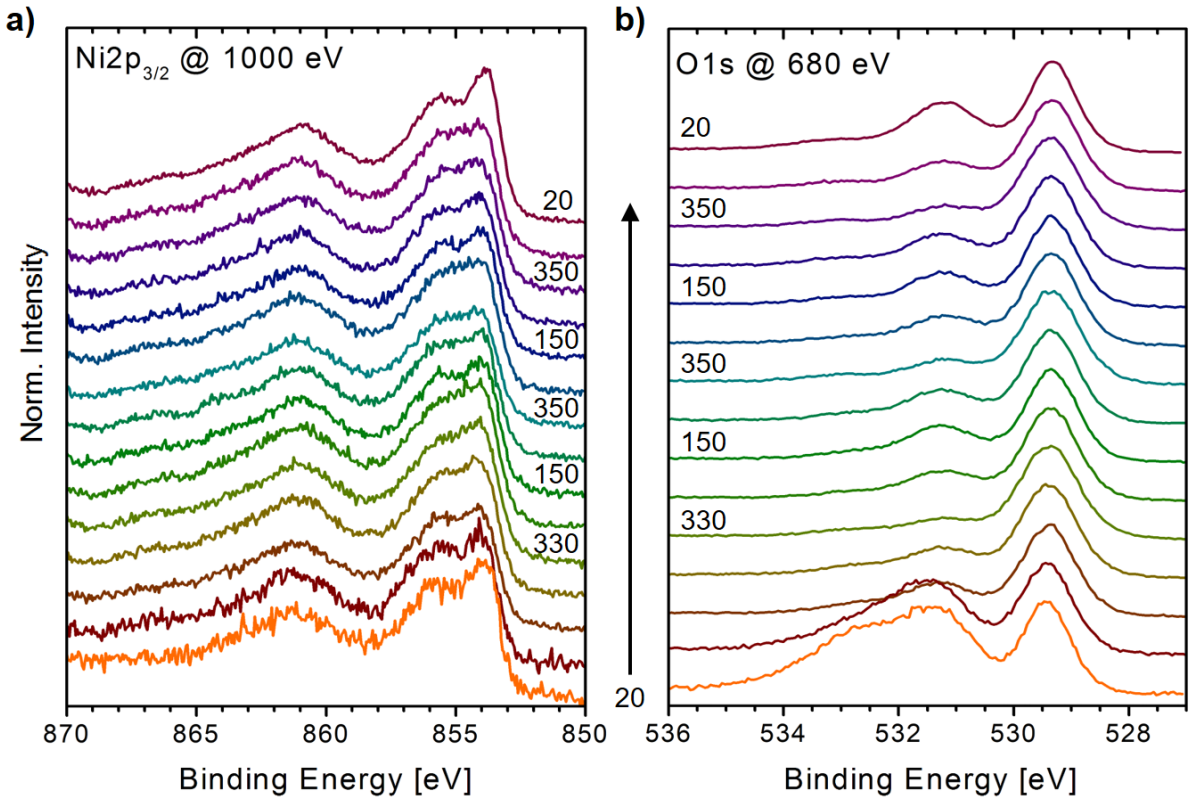

SI-Figure 5: a) $Ni2p_{3/2}$ spectra during heating-cooling cycles in 0.5 mbar O_2 atmosphere. b) O1s spectra corresponding to a). The same color indicates the same temperature in each region.

SI-Figure 5 shows the complete $Ni2p_{3/2}$ and O1s data sets recorded during three heating-cooling cycles in 0.5 mbar O_2 atmosphere corresponding to Figures 4 and 5 of the main text.

XAS: Reconstruction of O K-edge

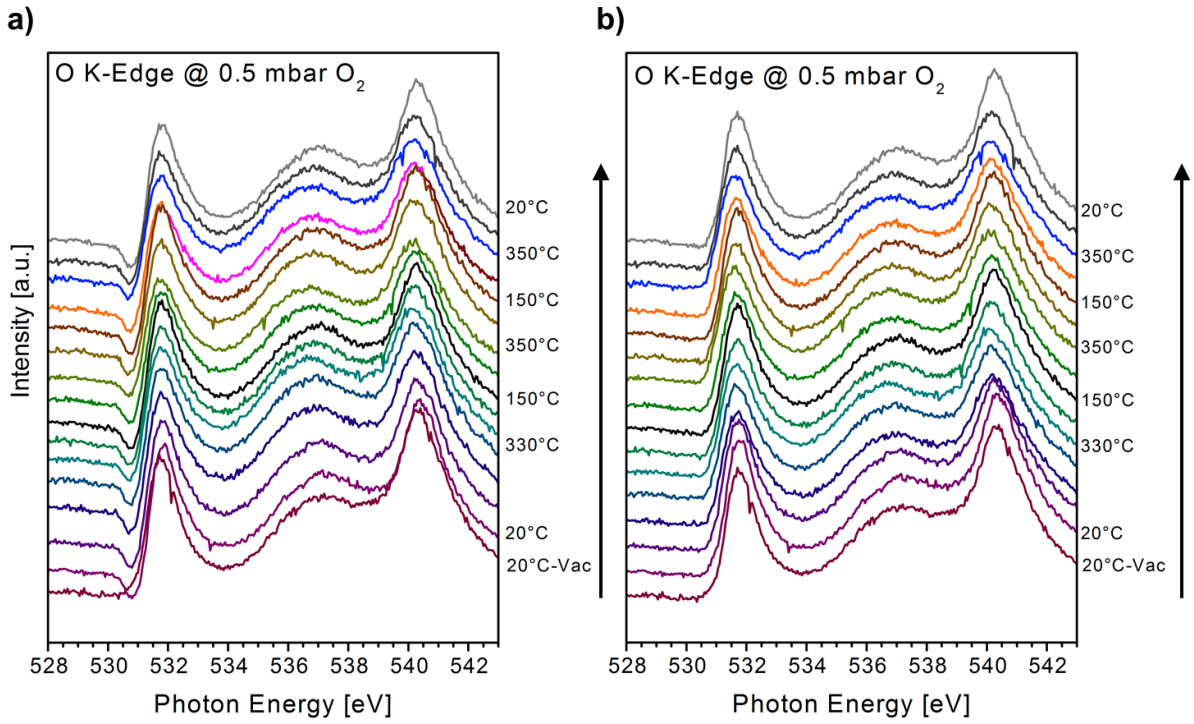

SI-Figure 6: a) As recorded O K-edge Auger Yield spectra taken during heating-cooling cycles in 0.5 mbar O_2 atmosphere. b) Reconstructed O K-edge spectra of a).

SI-Figure 6 shows the complete set of XAS data recorded during three heating-cooling cycles in 0.5 mbar O_2 atmosphere. In SI-Figure 6 a) in the measured spectra at a photon energy of ≈ 531 eV a distinct intensity loss is visible which stems from the π^* absorption resonance in the O_2 gas phase. By applying a reconstruction procedure, developed by Hävecker et al. and described in detail in reference [22], this feature can be removed as displayed in SI-Figure 6 b) and in Figure 6 b) and c) of the main text. In short, in this procedure, the measured spectrum is normalized to the inverted and appropriately scaled, gas phase dominated Total Electron Yield spectrum. The latter can be considered as a measure of the absorption of light in the gas on the way towards the sample surface causing the intensity loss at ≈ 531 eV.

The quality of the procedure can be validated by comparing the reconstructed spectra recorded in 0.5 mbar O_2 atmosphere to their counterparts recorded in vacuum and in 0.5 mbar H_2O atmosphere, respectively. The latter is particularly suited because a) no gas phase absorption is distorting those spectra and b) the effect of oxygen vacancy formation is affecting the spectral shapes in a very similar fashion in dependence of temperature as in O_2 atmosphere. We will address this in detail in the second part of our studies of the role of oxygen vacancies in OH - bond formation on NiO_x.[23] As an example, SI-Figure 7 compares the low energy side of spectra recorded in vacuum (only at 20°C) and 0.5 mbar H_2O atmosphere at 20°C and 350°C, respectively, to the reconstructed spectra recorded at the same temperatures in 0.5 mbar O_2 atmosphere. The spectra taken at 20°C all agree well with each other (SI-Figure 7 a). Similarly, after heating to 350°C as shown in SI-Figure 7 b), both, the O_2 - as well as the H_2O – related spectrum, exhibit the same broadening with respect to the 20°C - vacuum spectrum as expected from the formation of oxygen vacancies as described in the main text.

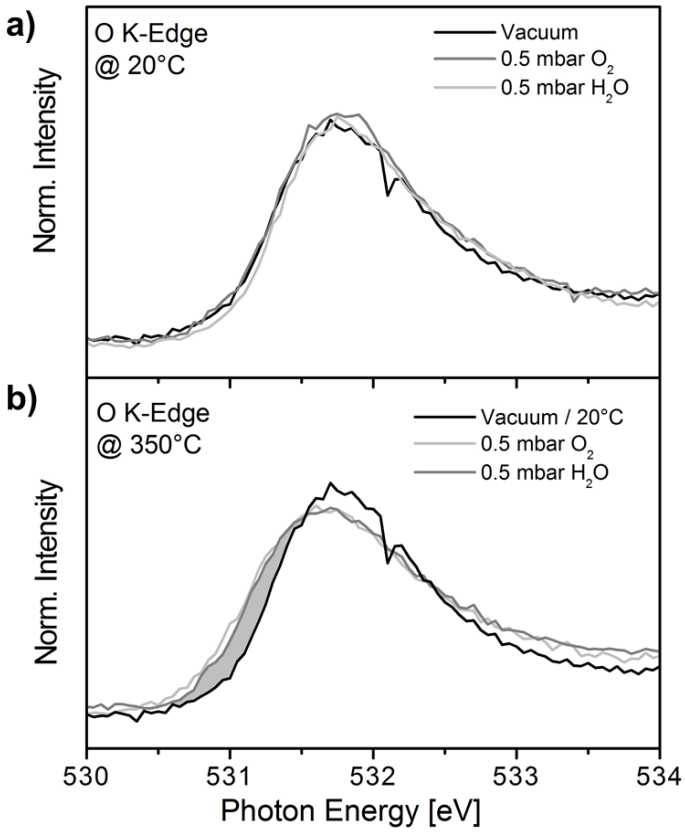

SI-Figure 7: a) Reconstructed O K-edge Auger Yield spectrum recorded in 0.5 mbar O_2 atmosphere at 20°C compared to its vacuum and 0.5 mbar H_2O counterparts. b) Reconstructed O K-edge Auger Yield spectrum recorded in 0.5 mbar O_2 atmosphere at 350°C compared to its 0.5 mbar H_2O- 350°C counterpart and the spectrum recorded at 20°C in vacuum.

XPS depth profiling during formation and replenishing of oxygen vacancies on NiO_x in O_2 atmosphere

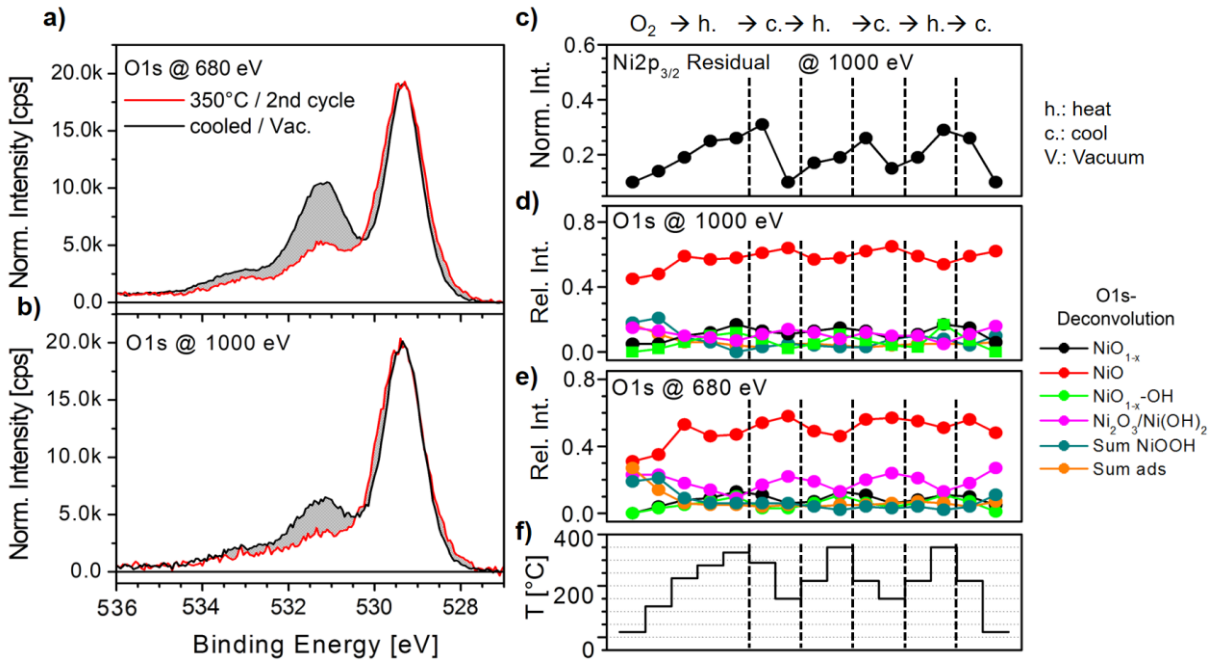

SI-Figure 8: a) and b) O1s spectra at 350°C in O_2 atmosphere and in vacuum after cooling recorded at photon energies of 680 eV and 1000 eV, respectively. For better comparison of the peak shapes the spectra are normalized. c) Evolution of the $Ni2p_{3/2}$ residual intensity derived from subtracting the fit of pure NiO from the measured spectrum. d) and e) Evolution of the relative intensities derived from the deconvolution of O1s spectra in dependence of temperature recorded at photon energies of 1000 eV and 680 eV, respectively. For better comparison of the O1s the components of both, NiOOH related peaks as well as both peaks assigned to adsorbats, are summarized. f) Heating profile.

SI-Figures 8 a) – e) show a comparison of the evolution of O1s spectra during heating-cooling cycles at different photon energies together with the evolution of the $Ni2p_{3/2}$ residual obtained from subtracting a fitted pure NiO spectrum from the respective measured spectrum. Apparently, closer to the surface, i.e., at lower photon energies, the broadening of the main NiO line at high temperatures as well as the spectral intensities at higher BEs and low temperatures are more pronounced (SI-Figures 8 a) and b). This also becomes obvious when following the progression of the relative intensities of the fitted O1s peaks. With respect to the intensity of the main NiO peak, the relative intensities of all peaks related to vacancies are higher for the surface sensitive (680 eV) than for the depth sensitive experiment (1000 eV) as can be seen in SI-Figures 8 d) and e), respectively. This depth profiling indicates that the oxygen vacancy formation is mostly a surface related process.

Work Function

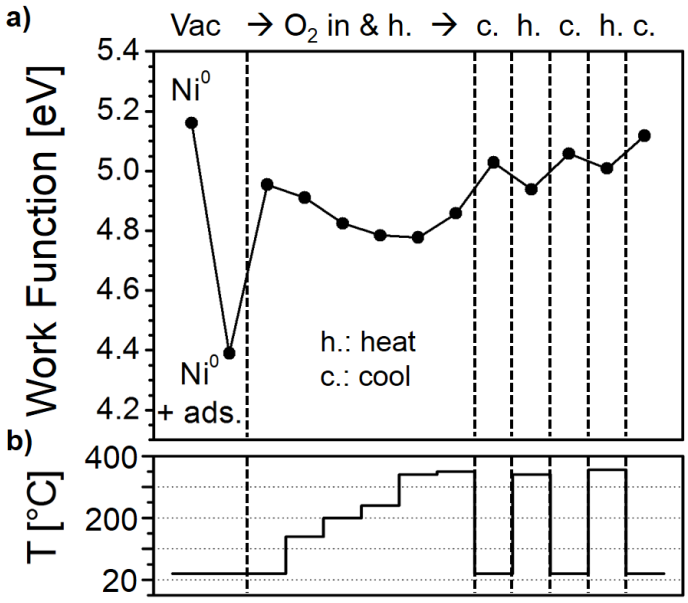

SI-Figure 9: a) Evolution of the work function recorded during heating–cooling cycles of a NiO_x film between RT and ≈ 350°C in 0.5 mbar O_2 atmosphere. b) Heating profile.

The work function (WF) was monitored during oxidation of metallic Ni and subsequent heating-cooling cycles as shown in SI-Figure 9. After removal of a native oxide layer on a fresh, air exposed Ni film the WF is as high as 5.15 eV which rapidly decreases by accumulating residual gas adsorbates within ≈ 8 hours in vacuum. (Note that the significant decrease of the WF of metallic Ni upon adsorption of residual gas, e.g., water or carbonaceous species has been observed before (e.g. [24]) Exposure to 0.5 mbar of oxygen atmosphere reverses most of this effect already at RT. During subsequent heating, the WF decreases again between 20 and 240°C and increases with further heating up to 350°C. Since oxidation roughly sets in between 150 and 200°C we can safely assume that the oxidation of Ni is responsible for the initial decrease. The surface may become rougher than the pristine Ni^0 surface due to the gradual formation of NiO_x islands. This increase of surface roughness is expected to lower the WF.[25] After full oxidation of Ni to NiO_x at 350°C and subsequent cooling to 20°C the WF measured in O_2 atmosphere is 5.0 eV which is in the expected range.[24,26,27] During the following heating-cooling cycles the WF alternates between higher values at low temperatures and lower values at high temperatures. For NiO_x a WF increase is expected in the presence of electronegative species, which, in our case, is provided by Ni vacancies prominently present at RT (see Figures 1, 2 b) and d) and 4 a) and c). In contrast, with the vanishing of Ni vacancies and the formation of oxygen vacancies at T ≥ 340°C the electronegativity is decreased leading to a decrease of the WF by ≈ 0.1 eV. This value is significantly smaller than the WF-decrease of 1.4 eV observed during partial reduction of NiO by Greiner et al.[24] However, in the present case the “partial reduction” is limited to the formation oxygen vacancies only leading to a small WF change. During the heating-cooling cycles a small overall increase of the WF is visible. This may be related to the formation of small amounts of NiOOH (see Figures 3 c) and 5 c) which reportedly increases the WF above the NiO_x value,[28] but it could also stem from further, undetected structural changes. A detailed description of the changes of the work function during heating-cooling cycles is given in the discussion in the main text.

[1] D. A. Shirley, *Phys. Rev. B* **1972**, 5, 4709-4714.
[2] S. Doniach, M. Sunjic, *J. Phys. C: Solid State Phys.* **1970**, 3, 285-291.
[3] M. C. Biesinger, B. P. Payne, A. P. Grosvenor, L. W. M. Lau, A. R. Gerson, R. St. C. Smart, *Appl. Surf. Sci.* **2011**, 257, 2717-2730. ([31] of main text.)
[4] A. P. Grosvenor, M. C. Biesinger, M. C., R. St. C. Smart, N. S. McIntyre, *Surf. Sci.* **2006**, 600, 1771-1779. ([32] of main text.)
[5] M. Fingerle, S. Tengeler, W. Calvet, T. Mayer, W. Jaegermann, *J. Electrochem. Soc.* **2018**, 165(4), H3148-H3153. ([19] of main text.)
[6] J. J. Yeh, I. Lindau, *Atomic Data and Nuclear Data Tables* **1985**, 32, 1-155.
[7] M. P. Seah, *Surface and Interface Analysis* **1986**, 9, 85-98.
[8] B. Frank, R. Blume, A. Rinaldi, A. Trunschke, R. Schlögl, *Angewandte Chemie, Int. Ed.* **2011**, 50, 10226-10230.
[9] S. Reiche, R. Blume, X. C. Zhao, D. Su, E. Kunkes, M. Behrens, R. Schlögl, *Carbon* **2014**, 77, 175-183.
[10] R. S. Weatherup, C. Baehtz, B. Dlubak, B. C. Bayer, P. R. Kidambi, R. Blume, R. Schlögl, S. Hofmann, *Nano Lett.* **2013**, 13, 4624-4631.
[11] R. S. Weatherup, B. C. Bayer, R. Blume, C. Baehtz, P. R. Kidambi, M. Fouquet, C. T. Wirth, R. Schlögl, S. Hofmann, *Chem. Phys. Chem.* **2012**, 13, 2544-2549.
[12] H. Kuhlenbeck, G. Odörfer, R. Jaeger, G. Illing, M. Menges, Th. Mull, H.-J. Freund, *Phys. Rev. B* **1991**, 43, 1969-1986. ([16] of main text.)
[13] M. Napari, T. N. Huq, R. L. Z. Hoye, J. L. MacManus-Driscoll, *InfoMat.* **2020**, 3, 1-41. ([18] of main text.)
[14] M. Sterrer, H.-J. Freund, in *Surface and Interface Science,* Vol. 3 (Ed.: K. Wandelt), Wiley-VCH, Weinheim, **2013**, pp. 229-278.
[15] M. A. Langell and M. H. Nassir, *J. Phys. Chem.* **1995**. 99, 4162-4169.
[16] M. A. Munoz-Marquez, R. E. Tanner, D. P. Woodruff, *Surf. Sci.* **2004**, 565, 1-13.
[17] L. Liu, S. Wang, S. Liu, Q. Guo, J. Guo, *Surf. Sci.* **2018**, 667, 8–12.
[18] N. Kitakatsu, V. Maurice, C. Hinnen, P. Marcus, *Surf. Sci.* **1998**, 407, 36-58. ([21] of main text.)
[19] V. Patil, S. Pawar, M. Chougule, P. Godse, R. Ratnakar, S. Sen, P. Joshi, *J. Surf. Eng. Mater. Adv. Technol.* **2011**, 1, 35-41. ([13] of main text.)
[20] M. S. Jamal, S. A. Shahahmadi, P. Chelvanathan, H. F. Alharbi, M. R. Karim, M. A. Dar, M. Luqman, N. H. Alharthi, Y. S. Al-Harthi, M. Aminuzzaman, N. Asim, K. Sopian, S. K. Tiong, N. Amin, Md. Akhtaruzzaman, *Results Phys.* **2019**, 14, 102360. ([14] of main text.)
[21] Z. Luo, L. Liu, X. Yang, X. Luo, P. Bi, Z. Fu, A. Pang, W. Li, Y. Yi, *ACS Appl. Mater. Interfaces* **2020**, 12, 39098-39107. ([15] of main text.)
[22] M. Hävecker, M. Cavalleri, R. Herbert, R. Follath, A. Knop-Gericke, C. Hess, K. Hermann, R. Schlögl, *Phys. Status Solidi B* **2009**, 246, 1459–1469.
[23] R. Blume, W. Calvet, A. Ghafari, T. Mayer, A. Knop-Gericke, R. Schlögl, submitted to *PCCP* **2023**.
[24] M. T. Greiner, M. G. Helander, Z.-B. Wang, W.-M. Tang, Z.-H. Lu, *J. Phys. Chem. C* **2010**, 114, 19777–19781. ([43] of main text.)
[25] R. Smoluchowski, *Phys. Rev.* **1941**, 60, 661-674.
[26] T. Dutta, P. Gupta, A. Gupta, J. Narayan, *J. Phys. D: Appl. Phys.* **2010**, 43, 105301. ([44] of main text.)
[27] J. Y. Zhang, W. W. Li, R. L. Z. Hoye, J. L. MacManus-Driscoll, M. Budde, O. Bierwagen, L. Wang, Y. Du, M. J. Wahila, L. F. J. Piper, T.-L. Lee, H. J. Edwards, V. R. Dhanak, K. H. L. Zhang, *J. Mater. Chem. C* **2018**, 6, 2275-2282. ([45] of main text.)
[28] K. X. Steirer, P. F. Ndione, N. E. Widjonarko, M. T. Lloyd, J. Meyer, E. L. Ratcliff, A. Kahn, N. R. Armstrong, C. J. Curtis, D. S. Ginley, J. J. Berry, D. C. Olson, *Adv. Energy Mater.* **2011**, 1, 813–820. ([47] of main text.)